Engineering Applications of Artificial Intelligence 113 (2022) 104959

Contents lists available at ScienceDirect

Engineering Applications of Artificial Intelligence

journal homepage: www.elsevier.com/locate/engappai

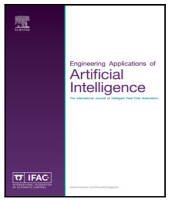

An efficient fault classification method in solar photovoltaic modules using transfer learning and multi-scale convolutional neural network

Deniz Korkmaz [a], Hakan Acikgoz [b,*]

[a] Malatya Turgut Ozal University, Faculty of Engineering and Natural Sciences, Department of Electrical and Electronics Engineering, Malatya, Turkey
[b] Gaziantep Islam Science and Technology University, Faculty of Engineering and Natural Sciences, Department of Electrical and Electronics Engineering, Gaziantep, Turkey

ARTICLE INFO

Keywords:
Solar energy
PV modules
Fault classification
Convolutional neural network
Transfer learning

ABSTRACT

Photovoltaic (PV) power generation is one of the remarkable energy types to provide clean and sustainable energy. Therefore, rapid fault detection and classification of PV modules can help to increase the reliability of the PV systems and reduce operating costs. In this study, an efficient PV fault detection method is proposed to classify different types of PV module anomalies using thermographic images. The proposed method is designed as a multi-scale convolutional neural network (CNN) with three branches based on the transfer learning strategy. The convolutional branches include multi-scale kernels with levels of visual perception and utilize pre-trained knowledge of the transferred network to improve the representation capability of the network. To overcome the imbalanced class distribution of the raw dataset, the oversampling technique is performed with the offline augmentation method, and the network performance is increased. In the experiments, 11 types of PV module faults such as cracking, diode, hot spot, offline module, and other classes are utilized. The average accuracy is obtained as 97.32% for fault detection and 93.51% for 11 anomaly types. The experimental results indicate that the proposed method gives higher classification accuracy and robustness in PV panel faults and outperforms the other deep learning methods and existing studies.

1. Introduction

As the continuous consumption of fossil fuels has caused serious diseases, environmental pollution, and distributing the ecological balance, renewable energy sources (RESs) such as solar, wind, hydroelectric, and geothermal energy have started to attract great attention all over the world (Acikgoz, 2022; Korkmaz, 2021; Korkmaz et al., 2021). Apart from the ecological effects, the global demand for electrical energy production and consumption has also increased the interest of RESs. Therefore, the use of renewable and low-carbon energy sources plays a significant role in supplying electrical energy demands for sustainable and environmentally friendly energy production (Ahmed et al., 2021; Ali et al., 2020). One of the remarkable and clean RES types is solar energy systems. Solar energy systems have the global primary energy demand of approximately 24% and have led to increasing global renewable energy investment accounting for 57% of the global investment in recent years (Rahaman et al., 2020). Solar power generation is generally provided with photovoltaic (PV) systems. PV systems have also drawn attention with their advantages such as being environmentally friendly, safe energy production, noiseless operation, and low installation costs (Li et al., 2021; Tang et al., 2020). While the annual average growth rate of solar energy is 50.2% between 2007 and 2017, the International Renewable Energy Agency reported that the global installed capacity of PV systems reached 400 GW in 2017 and 580 GW in 2019, showing an average increment of 45% in just two years (Acikgoz, 2022; Rahaman et al., 2020). Consequently, the installation of PV generation plants has been rapidly increasing every year, and investors, governments, and international organizations have a rapid adoption in PV power plants.

In PV plants, losses of electricity production are generally caused by the presence of various anomalies influencing the operation systems. These anomalies cause both reduced efficiency and electrical risks for operators in PV systems (Ali et al., 2020; Manno et al., 2021). The various anomalies also seriously affect the reliability and safety of the system operation (Cai et al., 2022, 2021, 2020). As PV systems are exposed to the harsh outdoor environmental effects, PV modules can be adversely affected by weather conditions such as temperature, rain, wind, etc., or by mechanical damages during transportation and installation. These damages could shorten the lifetime of the PV modules. In addition, environmental pollution by heavy metals may occur due to the discharge of PVs, which adversely affects recycling in nature (Aziz et al., 2020; Le et al., 2021). Therefore, automatic anomaly detection of PV modules in PV power plants ensures correct maintenance and fast

* Corresponding author.
E-mail addresses: deniz.korkmaz@ozal.edu.tr (D. Korkmaz), hakan.acikgoz@gibtu.edu.tr (H. Acikgoz).

https://doi.org/10.1016/j.engappai.2022.104959
Received 4 January 2022; Received in revised form 29 April 2022; Accepted 9 May 2022
Available online 21 May 2022

detection of plant faults and is a key solution to increase the reliability and durability of power generation (Haque et al., 2019; Rico Espinosa et al., 2020).

In recent years, various studies have been examined to classify anomalies of PV panel faults. Existing studies can be divided into two main groups as use of electrical measurements to detect faults (Aziz et al., 2020; Dhibi et al., 2020) and the use of thermography images for visual inspection (Fonseca Alves et al., 2021; Kirsten Vidal de Oliveira et al., 2020). Electrical measurement-based approaches are performed with a variety of methods, the most popular of which are model-based analysis and data-driven methods (Li et al., 2021). However, some failures that may occur in PV panels cause changes in current–voltage (I–V) curves that can hardly be detected. While this makes anomaly classification difficult, it also increases the time-consuming and installation cost of the fault detection system (Fernández et al., 2020; Huerta Herraiz et al., 2020; Tang et al., 2020). The use of visual anomaly classification makes it more simplify the monitoring and maintenance of the systems and provides low operation costs (Fonseca Alves et al., 2021; Le et al., 2021). With the development of artificial intelligence, deep-learning-based automatic detection and classification of anomalies from thermographic PV images has become more efficient and accurate (Huerta Herraiz et al., 2020; Manno et al., 2021; Otamendi et al., 2021). On the contrary machine learning techniques, deep learning has higher feature extraction and learning capabilities to achieve more accurate and robust classification performance. In addition, deep learning models can provide nonlinear representation and generalization capabilities for big data.

Different studies about PV panel fault detection and classification have been proposed in the literature. Ali et al. (2020) proposed a hybrid features-based support vector machine (SVM) model using infrared thermography technique for hotspot detection and classification into three different classes as healthy, non-faulty hotspot, and faulty. The hybrid feature vector consisting of RGB, texture, the histogram of oriented gradient, and the local binary pattern was formed using a data fusion approach. The experimental results gave in 96.8% training accuracy and 92% testing accuracy. Tang et al. (2020) proposed a convolutional neural network (CNN) model-based fault detection of PV modules using a large number of high-quality electroluminescence image generation methods for the limit of samples. Conventional image processing and the generative adversarial network characteristics were used for the image generation method. The results obtained as 84%, 82%, 81%, and 83% of accuracies for defect-free, micro-crack, finger-interruption, and break defect types, respectively. Manno et al. (2021) designed a CNN model for the automatic classification of thermographic images into two classes as a hotspot and operating. Various pre-processing techniques were also evaluated to reduce image noise. Considering a dataset that refers to different acquisition protocols, they reached a model accuracy of 99%. Le et al. (2021) designed a deep neural network model to classify solar module anomalies using thermographic images in the same unbalanced dataset. A residual network structure and ensemble technique were used to design the classification network. The results achieved an average accuracy of 94% and correctly classify twelve anomaly types on an average of 86%. Rico Espinosa et al. (2020) proposed an automatic fault classification method for PV plants using CNNs for semantic segmentation and classification from RGB images. The results were obtained an average accuracy of 75% for two classes as a fault and no-fault, and 70% for four classes as no-fault, cracks, shadows, and dust. Fonseca Alves et al. (2021) proposed a CNN-based fault detection method to classify eleven different anomaly classes in PV modules through thermographic images in an unbalanced dataset. The effect of data augmentation techniques was investigated to increase the performance of the designed method. Through a cross-validation method, the testing accuracy was obtained as 92.5% for the anomaly detection and 78.85% to classify defects for eight selected classes. In another study, a region-based CNN model was designed and relative hot regions were detected with an accuracy of 99.02% (Huerta Herraiz et al., 2020). Otamendi et al. (2021) proposed an end-to-end deep learning approach to detect, locate and segment cell level anomalies with an average accuracy of 84% for defective and non-defective classes. A deep learning and feature-based approach to detect and classify defective photovoltaic modules using thermal infrared images in a South African setting were analyzed by Dunderdale et al. (2020). The scale-invariant feature transform (SIFT) descriptor combined with a random forest classifier was used to identify defective photovoltaic modules. The feature-based methodology achieved an accuracy of 91.2% between defective and non-defective modules. Wang et al. (2021) integrated image processing and statistical machine learning techniques for online analysis of the raw video streams of aerial thermography. The transform invariant low-rank textures (TILT) method was used to crop out the background and the robust principal component analysis (RPCA) was applied to separate sparse corrupted anomalous components from a low-rank background. The authors detected the anomalies with a sensitivity of 80%. Cipriani et al. (2020) developed an innovative approach by a CNN model to classify the dust and hotspot anomalies related to photovoltaic systems through the use of thermographic images. They distinguished the hotspot conditions from the dust with an accuracy of 98%. In another study, ResNet-50 was used to classify ten common module anomalies from thermographic UAV videos. They handled the large amounts of thermographic images acquired during inspection of PV plants, extracted individual PV modules, and classified with an accuracy of more than 90% (Bommes et al., 2021). According to the current literature, deep learning-based models, especially CNNs, provide appropriate classification results. However, there are some open topics. First, the classification accuracies have not still superior for PV module anomalies and the average classification accuracies should be improved by over 90% for multi-class anomalies. Secondly, many studies have focused on datasets with either 2-class (Anomaly/No-Anomaly), 3-class, or 4-class. As the PV panels could be affected by harsh outdoor environments, there can occur various types of anomalies as cracking, diode, multi diode, hot spot, multi hot spot, soiling, vegetation, and etc. Therefore, extensive datasets can still be studied by designing new types of CNNs to increase the number of anomaly classes and their accuracy performance.

To bridge the aforementioned gaps in the current literature, a novel and effective multi-scale CNN architecture-based PV anomaly detection method to classify PV module faults is proposed in this paper. This architecture classifies the different types of damages in the PV modules using a thermographic image dataset collected from real large-scale PV farms. The dataset is one of the largest publicly available datasets that includes 11 types of anomalies as cracking, diode, hot spot, soiling, vegetation, and other classes. The multi-scale CNN model combines the transfer learning strategy with a designed three-branched structure. Since low-level convolutions have small-sized filters, two new convolutional branches are proposed and connected to low-level convolutions in parallel. The branch structure includes low, middle, and high-level convolutional kernel sizes to extract multiple-scale spectral features from the input images with few self-parameters and strong generalization ability. Subsequently, the obtained features are concatenated as the subset feature vector and fed to the last low-level convolution to reduce the output dimension. The proposed CNN model is based on the AlexNet architecture and utilizes its representation capability. The main reason for using this model is that it provided successful performance in ImageNet challenging competition. In addition, the oversampling method is performed with offline augmentation to overcome the imbalanced class distribution of the raw dataset and increase the generalization capability of the network performance. In the experiments, the obtained results are compared with various deep learning methods and the existing state-of-the-art studies to evaluate the effectiveness of the proposed method. As a result, this study contributes to the existing literature by emphasizing the effectiveness of the multiple-scale feature extraction, the improvement of the network performance with offline augmentation, and increasing the performance of the fault

classification in PV modules on the largest multi-class dataset. **The novelty and main contributions of this paper can be summarized as follows:**

- **A novel multi-scale CNN model is proposed to achieve robust and high classification performance in PV panels.** The proposed method is a combination of the transfer learning strategy with a designed three-branched structure. Therefore, convolutional kernels can extract multiple-scale deep features with different levels of visual perception. This structure gives the competitive accuracy improvement to classify large-scale anomaly classes in PV modules through thermographic images. The proposed method also outperforms related existing studies.
- **The proposed method is validated with different solar PV plants.** Although most of the literature studies focus on the analysis of individual PV panels or plants, the used publicly available dataset was collected from 6 continents and includes real-world infrared PV images. Therefore, the generalization capability of the proposed method is increased.
- **The frequently encountered faults in PV modules operating in an array are identified and classified.** Many studies have only focused on 2-class (Anomaly/No-Anomaly), 3-class, or 4-class. However, common panel faults in PV systems could be caused by multiple cells, diodes, and hotspots. Blocked sunlight, vegetation, and soiling also negatively affect the operation of panels. Hence, the comprehensive classification is performed with 11 types of faults and No-Anomaly classes.

The remainder of the paper is structured as follows: Section 2 presents the materials and methods with details of the dataset description, the general framework of the proposed method, CNN architecture, and dataset improvement with augmentation. In Section 3, the experiments, findings of the study, and comparisons are given. Finally, the conclusion of the study is briefed in Section 4.

2. Materials and methods

To prevent energy loss and provide early fault diagnosis in solar PV systems, an intelligent decision-making mechanism can be developed by using artificial intelligence-based approaches. Contrary to conventional machine learning algorithms, CNN architectures can give effective solutions to classification problems with their strong self-learning abilities and state-of-the-art performances. A convolutional network consists of a chain of convolutions, normalization operations, pooling layers, and dense layers. Convolution layers convolute their inputs using filters and transfer the outputs to the activation functions. Pooling layers reduce the dimension of the inputs coming from activations with a statistic of nearby cells. Therefore, more learned features can be extracted and the feature representation ability of the network can be improved (Manno et al., 2021). Considering these powerful features of CNNs, a novel and robust CNN-based PV fault classification method is proposed. The designed deep classification network aims to effectively classify thermographic panel anomalies by extracting distinctive visual properties. The proposed method may assist in providing reliable anomaly detections with consideration for the safety and economic operation of solar power systems. The following subsections present the dataset description, framework of the proposed method, multi-scale CNN architecture, and offline augmentation for network improvement in detail.

2.1. Infrared solar modules dataset description

There are many different faults that PV panels may encounter during the operation periods. The occurrence of insect traces, shadowing of panels due to buildings, vegetation formation, incompatibility of PV cells, panel cracks, diode failures, panel pollution, and diverse weather conditions such as snow are frequently encountered anomalies. Therefore, a distinctive and publicly available dataset namely the Infrared Solar Modules dataset (Matthew et al., 2020) is selected to provide a comprehensive classifier architecture. The dataset includes real-world thermographic infrared PV images of various anomalies found in solar systems. The data is collected by the Raptor Maps Inc team with piloted aircraft and unmanned aerial systems, using mid-wave and long-wave infrared (3–13.5 μm) camera modules. The resolution varies from 3.00 to 15.00 cm/pixel. Each anomaly is cropped to the individual module and the whole data is separated into twelve unique classes (Fonseca Alves et al., 2021).

The dataset contains 20,000 images with 24 × 40 resolution and 8-bit depth in one channel. There are 11 different anomaly classes and one nominal module (No-Anomaly) class. The dataset includes a total of 10,000 images for anomaly classes and 10,000 images for No-Anomaly class. Table 1 describes the dataset and number of each class. The number of anomaly samples varies from 175 to 1877 images in the dataset. While 50% of samples represent only nominal modules, the rest of the samples contain 11 different anomalies. Although the imbalanced structure of the class distribution is a major challenge for the classification, the proportion of the classes is determined by considering the total existing global findings. Therefore, the dataset contains a rich presentation of the related PV panel defects, faults, and findings. Fig. 1 shows the randomly selected image samples from the dataset. In this figure, it is noted that the samples are colored for only visualization. Some classes can be easily observed such as Cell, Hot-Spot, and Diode, while some are difficult to distinguish. Therefore, it is necessary to detect panel anomalies rapidly and easily with an effective network design without the need for expert intervention.

2.2. Framework of the proposed method

The general structure of the proposed PV anomaly classification method is presented in Fig. 2. The proposed method provides the classify faults in PV modules obtained from thermographic images and it consists of two main processes: offline data augmentation for the network improvement and transfer learning-based network training and testing. Although the used dataset includes a big part of 10,000 No-Anomaly class images, some classes have fewer samples. Therefore, offline augmentation is performed to prevent the imbalanced class distribution and increase the generalization capability of the network. The offline augmentation method is a sample duplication technique that increases the training set while preserving the original labels. Also, dataset initialization is employed for data split. Training and validation sets are set as the inputs of the training phase and the test set is used for the testing phase. After the pre-processing, transfer learning-based network architecture is constructed to extract multi-scale feature maps. For transfer learning, the pre-trained AlexNet architecture is used and two new branches with different convolutional kernel sizes are added. This approach can reuse the convolutional weight parameters of the pre-trained network to enhance the representation capability and classification accuracy.

For optimization of the network, the stochastic gradient descent (SGD) algorithm is performed to extract the convolutional kernels during the back-propagation process. After training, the multi-scale CNN model learns to extract high-level features to classify anomalies with strong representation capability.

2.3. Multi-scale CNN architecture

Although training a CNN from scratch requires a large data size, it is difficult to organize a large dataset of relevant problems. In many applications, CNNs have large initialized parameters and the related tasks may not have big data to prevent over-fitting. Training and testing data matching is also a complicated process. Therefore, transfer learning is widely used to aid optimize model performance. Transfer learning is

Table 1
Classes and anomaly descriptions (Matthew et al., 2020).

Class name	Number of images	Description
Cell	1877	Hot spot occurring with square geometry in single cell.
Cell-Multi	1288	Hot spots occurring with square geometry in multiple cells.
Cracking	940	Module anomaly caused by cracking on the module surface.
Diode	1499	Activated bypass diode, typically 1/3 of the module.
Diode-Multi	175	Multiple activated bypass diodes, typically affecting 2/3 of module.
Hot-Spot	249	Hot spot on a thin-film module.
Hot-Spot-Multi	246	Multiple hot spots on a thin-film module.
Offline-Module	827	The entire module is heated.
Shadowing	1056	Sunlight obstructed by vegetation, man-made structures, or adjacent rows.
Soiling	204	Dirt, dust, or other debris on surface of module.
Vegetation	1639	Panels blocked by vegetation.
No-Anomaly	10,000	Nominal solar module.
12-Class	**20,000**	**Total**

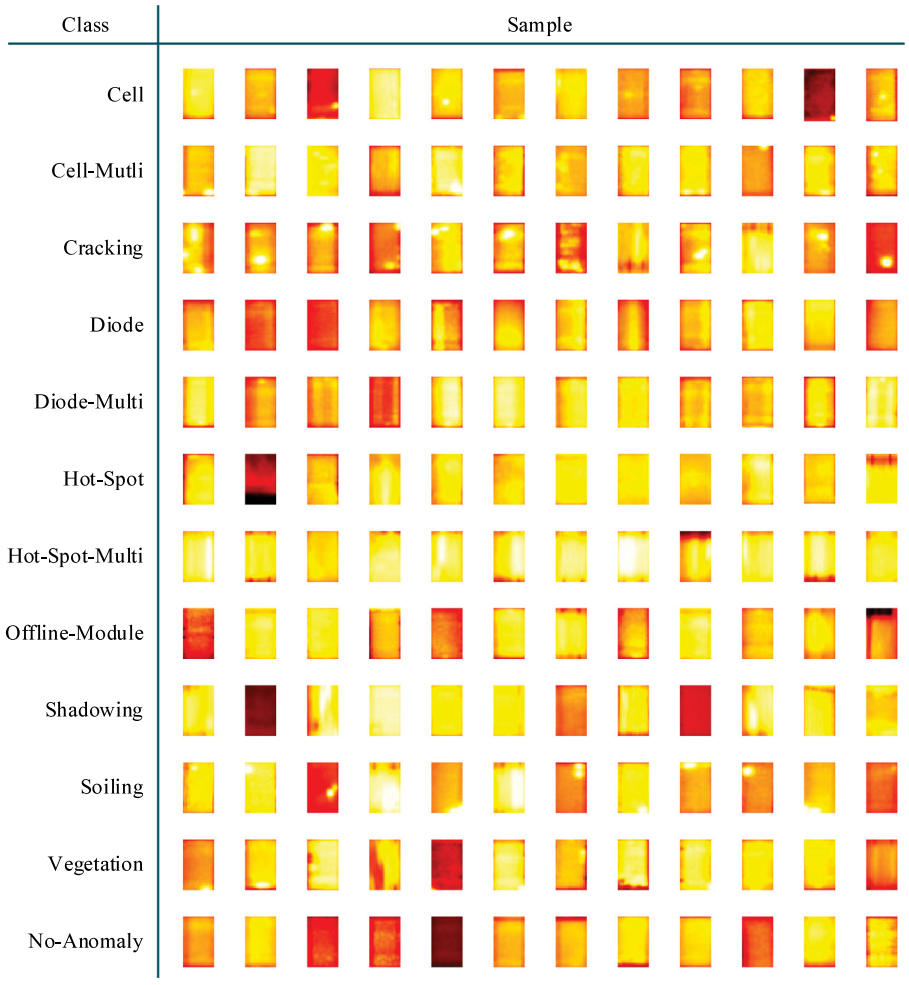

Fig. 1. Randomly selected class samples from the dataset.

one of the well-known methods in which knowledge obtained with an already-trained model is utilized to learn other relevant datasets (Han et al., 2018; Pan and Yang, 2010). Given a source domain, the base model is trained for a specific task (T_s) on its dataset (X_s) and then the trained model is transferred to the target task (T_t) to re-train with the target data (X_t) using the knowledge in T_s and X_s. According to the type and structure of the task, various model settings can be defined for this process (Deepak and Ameer, 2019; Pan and Yang, 2010). Based on the transfer learning strategy, a multi-scale CNN architecture is proposed to effectively classify PV panel anomalies in this paper.

As shown in Fig. 3, the proposed CNN model is designed by modifying the AlexNet architecture and utilizes its representation capability. AlexNet is an efficient CNN model in image recognition problems and it was proposed by Alex Krizhevsky et al. in the 2012 ImageNet Scale Visual Recognition Challenge (ILSVRC-2012) (Ballester and Araujo, 2016). The original AlexNet structure consists of twelve layers with five convolutional layers, three max-pooling, three fully-connected, and one classification layer. In the network, first two convolution layers utilize 11×11 and 5×5 while the next three convolutions use 3×3 kernel-sized filters. Max-pooling layers have only 3×3 kernels. However, the low-level convolution layers with 3×3 small-sized filters cannot obtain

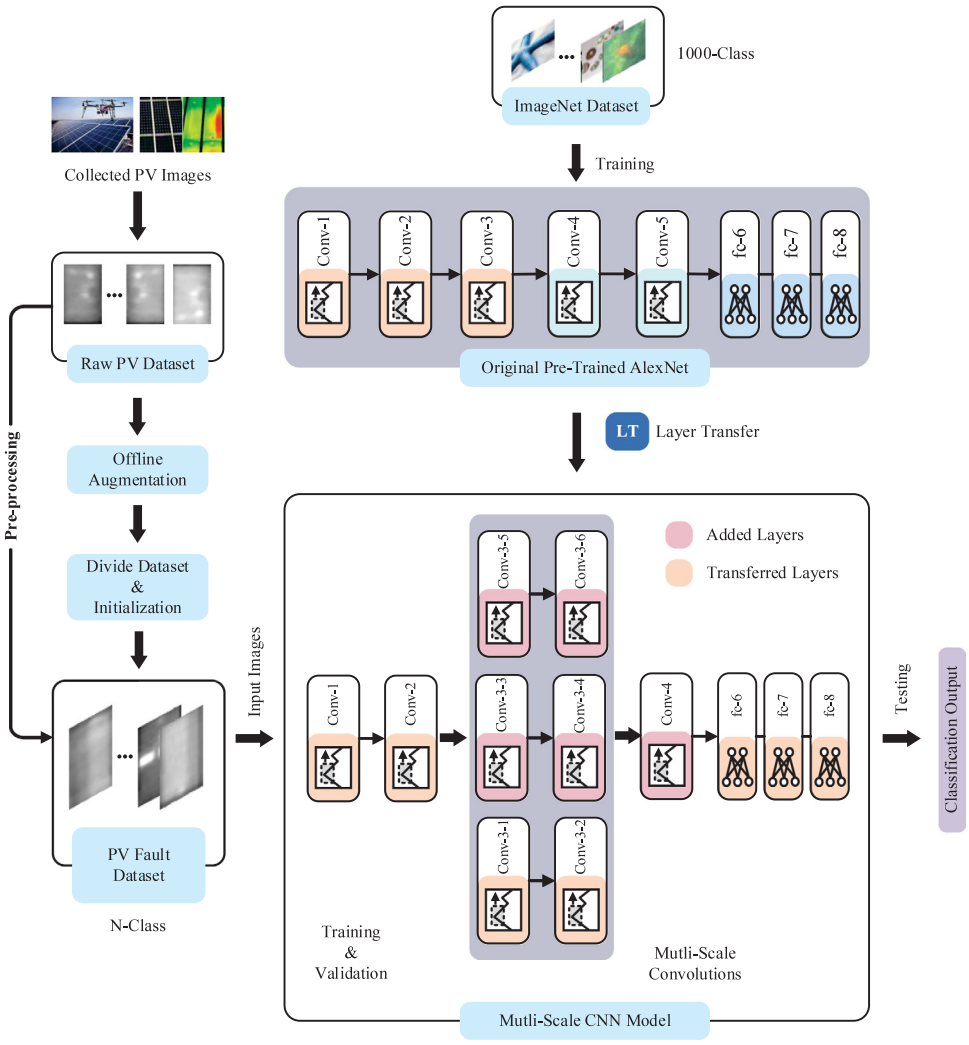

Fig. 2. The general structure of the proposed PV anomaly classification method.

sensitive features from the output of neurons in the deep layers for PV anomalies. Therefore, the pre-trained AlexNet architecture is modified to extract more detailed feature maps and a novel and efficient multi-scale CNN model is proposed. Since low-level convolutions have small-sized filters, two new convolutional branches are added to series-connected of 3 × 3 convolutional layers. These branches include middle and high level filter banks with 5 × 5 and 7 × 7 kernels to extract multi-scale spectral features from the inputs (Liu et al., 2021). Convolutions at the input layer {*Conv*-1(11, 96) – *Conv*-2(5, 256)} extract general input features and send the knowledge to the parallel branches. According to the input size of the AlexNet, the PV image set are resized to 227 × 227 pixels. The designed CNN architecture consists of three parallel branches with different sizes of convolutions as: {*Conv*3-1(3, 384) - *Conv*3-2(3, 384)} for fine-grained features with small-sized filters, {*Conv*3-3(5, 384) - *Conv*3-4(5, 384)} for middle-grained features with middle-sized filters, and {Conv3-5(7, 384) - Conv3-6(7, 384)} for coarse-grained features with large-sized filters, respectively. After these operations, three branches are concatenated into one feature map and it is sent to the last 1 × 1 convolutional layer *Conv*-4(1, 512) to reduce the output dimension and obtain multi-channel features.

For the convolutions, let m is the filter size of the jth layer n, b is the bias matrix, and K defines the kernel. Then, the output of the jth layer $y_{n,j}$ is expressed by;

$$y_{n,j} = f_a\left(\sum_{k=1}^{m_{j,n-1}} I_{k,n-1} \times K_{n,j} + b_{n,j}\right) \tag{1}$$

where $f_a(\cdot)$ is the activation function. In the network, convolutions are activated with ReLU functions to decompose the noises and improve the learning speed. The output of the ReLU function f is given by:

$$f_a(t) = \begin{cases} 0, & t < 0 \\ t, & t \geq 0 \end{cases} \tag{2}$$

At every depth change, one max-pooling layer is used to reduce the dimension of the features from the activation function with a statistic of nearby outputs, and it can be given by the following equation;

$$P_j = max\left(F^R\right) \Big| F = f_j \quad i \in R \tag{3}$$

Here, R is the pooling region. Finally, neurons of the first two fully-connected layers are set to 1000 and the last fully-connected layer gives the probability of the defined classes according to the anomalies. These layers obtain a deep feature vector. As given in Eq. (1), a fully-connected layer multiplies the input by a weight matrix w and appends to a bias vector:

$$Y_{n,j} = \sum_{k=1}^{m_{j,n-1}} Y_{k,n-1} \times w_{n,j} + b_{n,j} \tag{4}$$

In addition, the softmax and classification layers are discarded and new layers are connected to the last fully-connected layer. In the network, original pooling layers, activation functions, and five convolutions of the AlexNet are transferred and convolutional layers are updated during training. Table 2 summarizes the corresponding relationship

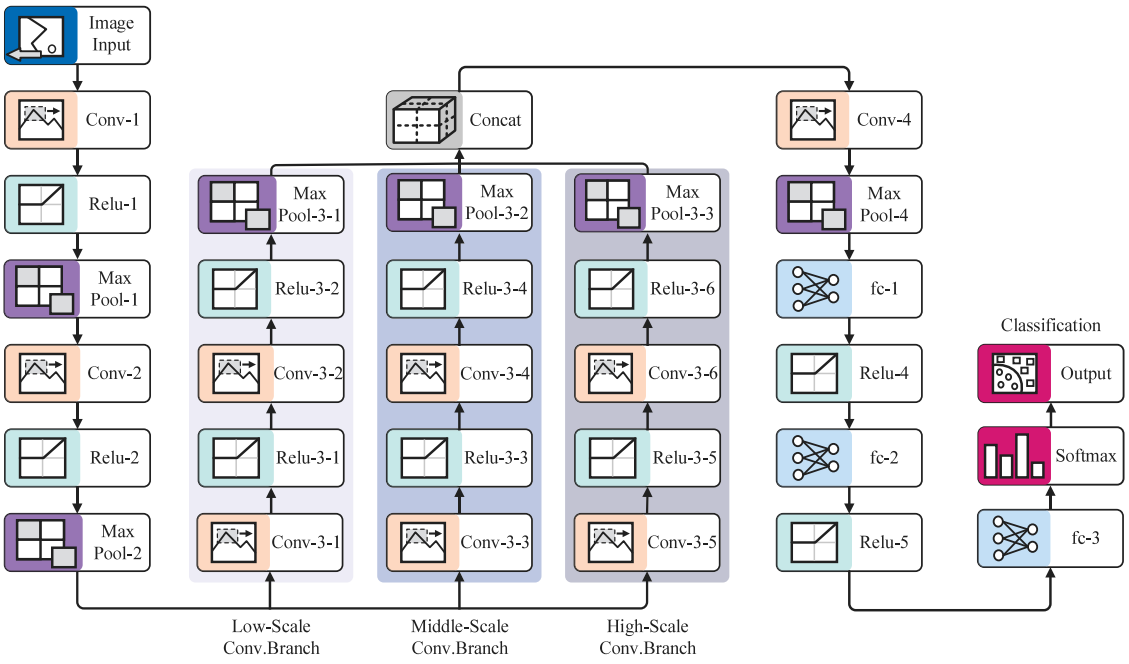

Fig. 3. Details on the design multi-scale CNN architecture.

Table 2
Relationship between the proposed network and AlexNet architecture. TL defines the transferred layers.

AlexNet	Multi-scale CNN		Description	Depth
Conv-1	Conv-1		TL	96
Conv-2	Conv-2		TL	256
Conv-3	Conv-3-1	Conv-3-2	Low-scale with TL	384
–	Conv-3-3	Conv-3-4	Adding middle scale	384
–	Conv-3-5	Conv-3-6	Adding high scale	384
–	Conv-4		Adding new layer	512
fc-6	fc-1		TL and Re-Organize	1000
ReLU-6	ReLU-4		TL	–
fc-7	fc-2		TL and Re-Organize	1000
ReLU-7	ReLU-5		TL	–
fc-8	fc-3		TL and Re-Organize	N-Class

between the designed network and AlexNet architecture. According to the network structures, the proposed method provides few learnable parameters compared to the AlexNet. While the original AlexNet has approximately 57M learnable parameters, the multi-scale CNN model has approximately 42M. Therefore, the proposed method not only improves the AlexNet but also provides the least number of learnable parameters.

As a result, the proposed CNN model with the parallel three branches makes it possible to extract multi-scale features from the input images with different scale knowledge. This architecture provides that the efficiency and representation capability of the network are increased through each filter in the branches concentrating on its own computation.

2.4. Offline augmentation for network improvement

In the classification problems of conventional machine learning and deep learning algorithms, the imbalanced class distribution of the dataset has a significantly negative impact on the model performances. The imbalanced ratio of the classes affects both the training convergences and the generalization capability of the trained model. The most commonly used solution is sampling the original images. Therefore, the balance of the classes can be increased. The sampling method can be divided into two strategies as oversampling and undersampling (Buda et al., 2018). In the oversampling, original images are augmented with artificial examples and a more comprehensive set of possible data points can be obtained. It also minimizes the distance between the class distributions. The undersampling method randomly removes from the majority classes and provides the same number of samples for all classes (Liu et al., 2021; Shorten and Khoshgoftaar, 2019).

The Infrared Solar Modules dataset used in this study is a huge dataset with 10,000 images representing different anomalies. However, the No-Anomaly class has 10,000 samples and it has 5.33 times more images than the second-largest Cell class. In addition, five classes have images under 1000 samples. Therefore, the oversampling method is performed with offline augmentation to overcome the imbalanced class distribution and increase the generalization capability. The key point in this stage is to keep the general point of view of the dataset. If an unsuitable augmentation is applied, the generated new samples do not represent the real world and do not contribute to the network performance. For this purpose, brightness, reversing, and rotation operations are selected to increase the number of samples. The brightness operation is used for decreasing and increasing the brightness of the images with ±30 to every pixel. Afterward, reversing and rotation operations are applied to original and resampled images. In the rotation, 180 degrees in a counterclockwise direction around the center point of the images are rotated. The reversing is applied two times with reversing the elements in each column and row. Therefore, 11 different samples from an original image are derived. Since the number of No-Anomaly class is quite large compared to other classes, all operations are applied to the anomaly classes while only rotation is used for the No-Anomaly class. As a result, each anomaly class size is increased 11 times and No-Anomaly class is increased 2 times in the training and validation sets. The number of images in the classes is offline augmented with the pre-processing of the dataset and an acceptable amount is obtained. An example aforementioned augmentation operation is given in Fig. 4 and the percentage distribution of raw and augmented classes is presented in Fig. 5 where the inner and outer loops represent the distributions before and after the augmentation. It should be noted that the undersampling method is also used for the 2-class classification process in the experiments to provide a balanced class distribution.

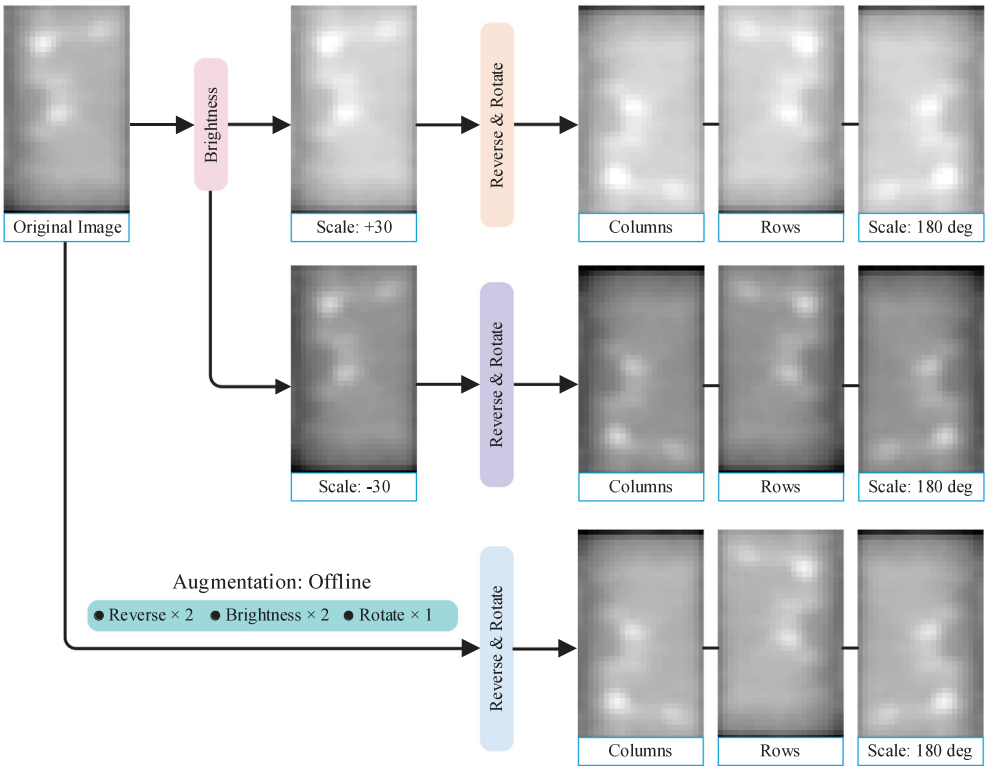

Fig. 4. Offline augmentation process of the images.

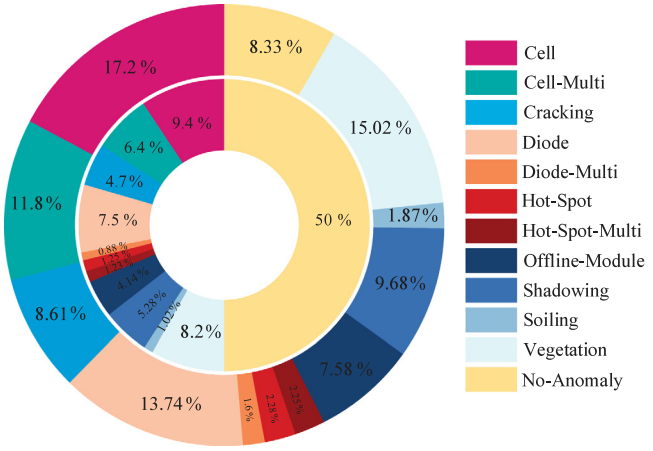

Fig. 5. Percentage distribution of images in the dataset for each class.

3. Experiments

In this section, experimental studies are carried out in order to analyze the statistical validity of the proposed method. Experimental studies are implemented in MATLAB® R2020b environment and performed on Intel (R) Core™ i7-10750H CPU @2.60 GHz, NVIDIA Quadro P620 GPU 16 GB RAM memory, and an x64-based processor. The remainder of this section presents the definitions of the benchmark networks and evaluation metrics. Moreover, experimental and improvement studies are performed in next section. Finally, the performance of the proposed method is compared with the state-of-the-art methods.

3.1. Benchmark networks

In order to verify the performance of the proposed method, the obtained results are compared with three different well-known deep networks as; AlexNet (Ballester and Araujo, 2016), SqueezeNet (Iandola et al., 2016), and ShuffleNet (Zhang et al., 2018). These networks are pre-trained CNNs for the extraction of deep intrinsic features and were trained on the ImageNet Large-Scale Visual Recognition Challenge dataset with 1000 different classes. AlexNet is an impressive CNN model that contains five convolution layers and three fully-connected layers (Ballester and Araujo, 2016). Contrary to AlexNet, SqueezeNet is an effective and smaller network with 50× fewer parameters AlexNet (Iandola et al., 2016). ShuffleNet contains pointwise group convolutions and shuffle operations to reduce computational complexity and assist the information transfer across channels (Zhang et al., 2018). In the experimental studies, the final layers of each network are redesigned according to the dataset classes and then retrained to classify new PV images. Therefore, they can be effectively utilized to perform PV anomaly classification problem by retraining.

3.2. Evaluation metrics

In order to quantitatively assess the performance of the proposed method, six evaluation metrics are used; Accuracy (Acc), Precision (Pr), Sensitivity (Sn), Specificity (Sp), F1-score (F1), and Matthew Correlation Coefficient (MCC). Acc gives the network performance for all classes. While Pr defines the truly positive results divided by the predicted positive results, Sn is the ratio of true positive results to all relevant samples. Sp measures the proportion of actual negatives that are predicted as negative. F1 gives the harmonic average with the combination of Pr and Sn. MCC also computes the differences between the actual and predicted classes. According to the obtained confusion matrix, these evaluation metrics are defined as follows:

$$\text{Acc} = \frac{N_{\text{TP}} + N_{\text{TN}}}{N_{\text{TP}} + N_{\text{FP}} + N_{\text{TN}} + N_{\text{FN}}} \tag{5}$$

$$\text{Pr} = \frac{N_{\text{TP}}}{N_{\text{TP}} + N_{\text{FP}}} \tag{6}$$

$$\text{Sn} = \frac{N_{\text{TP}}}{N_{\text{TP}} + N_{\text{FN}}} \tag{7}$$

Table 3
The classification results of all methods for 2-class.

Method	Acc (%)	Pr (%)	Sn (%)	Sp (%)	F1 (%)	MCC (%)
SqueezeNet	85.02	85.90	83.80	95.20	84.84	70.07
ShuffleNet	91.50	93.05	89.70	93.30	91.34	83.05
AlexNet	93.20	92.90	93.55	92.85	93.22	86.40
Proposed method	**97.32**	**97.63**	**97.00**	**97.65**	**97.32**	**94.65**

Table 4
The classification results of all methods for 11-class.

Method	Acc (%)	Pr (%)	Sn (%)	Sp (%)	F1 (%)	MCC (%)
SqueezeNet	75.15	75.87	75.15	97.52	74.50	72.65
ShuffleNet	82.94	82.95	82.94	98.29	82.74	81.16
AlexNet	85.02	85.36	85.02	98.50	84.60	83.46
Proposed method	**93.51**	**93.52**	**93.51**	**99.35**	**93.49**	**92.86**

$$\mathrm{Sp} = \frac{N_{\mathrm{TN}}}{N_{\mathrm{TN}} + N_{\mathrm{FP}}} \tag{8}$$

$$\mathrm{F1} = \frac{2 \times N_{\mathrm{TP}}}{2 \times N_{\mathrm{TP}} + N_{\mathrm{FP}} + N_{\mathrm{FN}}} \tag{9}$$

$$\mathrm{MCC} = \frac{\left(N_{\mathrm{TP}} \times N_{\mathrm{TN}}\right) - \left(N_{\mathrm{FP}} \times N_{\mathrm{FN}}\right)}{\sqrt{\left(N_{\mathrm{TP}} + N_{\mathrm{FP}}\right) \times \left(N_{\mathrm{TP}} + N_{\mathrm{FN}}\right) \times \left(N_{\mathrm{TN}} + N_{\mathrm{FP}}\right) \times \left(N_{\mathrm{TN}} + N_{\mathrm{FN}}\right)}} \tag{10}$$

In the equations, N_{TP}, N_{FP}, N_{TN}, and N_{FN} are the number of correctly classified anomalies, number of incorrectly classified anomalies, number of correctly classified opposite anomalies, and number of misclassified anomalies, respectively. Therefore, the correctness, effectiveness, and robustness of the proposed method can be analyzed with the above metrics.

3.3. Analyzes and results

In the experiments, the proposed multi-scale CNN method and pre-trained deep learning models are trained with the same dataset. While 80% of the dataset is used in training, the remaining dataset is equally used for testing and validation. In the training process, the input image size is 227 × 227, the mini-batch size is adjusted to 32 and the maximum epoch is preferred as 50. The learning rate is selected as 1e−3 and reduced by a drop factor of 0.5 after every 10 epochs. The training process of the proposed method is completed in a total of 50,000 iterations for 2-class and 28,850 iterations for 11-class. Fig. 6 demonstrates the training processes for 2-class and 11-class.

Experimental studies are separately carried out for both classes. For the 2-class experiments, the Anomaly and No-Anomaly labels are defined. Therefore, the first experiment represents whether there is an anomaly in the PV images. For the 11-class experiments, the Anomaly labeled images are divided according to the anomaly types and 11 different PV panel anomalies are analyzed. First, the experiments are performed for 2-class. After the data augmentation process, the dataset is comprised of a total amount of 123,668 images, including 103,668 anomaly images and 20,000 No-Anomaly images. An equal number of images are taken to balance both fault classes. The new dataset obtained for the 2-class consists of 20,000 Anomaly and 20,000 No-Anomaly.

First of all, the metric results obtained from the 2-class are presented in Table 3. As can be clearly seen from Table 3, while the classification accuracy values of the pre-trained deep learning methods are 85.02% for SqueezeNet, 91.50% for ShuffleNet, and 93.20% for AlexNet, the accuracy value of the proposed method is calculated as 97.2%. When all deep learning methods are analyzed in terms of their precision values, the proposed multi-scale CNN method gives the best value, which is 97.63%. On the other hand, those of SqueezeNet, ShuffleNet, and AlexNet are calculated as being 85.90%, 93.05%, and 92.90%, respectively. From these values, it can be clearly seen that the proposed method can make significant contributions to classification success.

When the proposed and pre-trained methods are compared in terms of their sensitivity values, the proposed method provides the best result while SqueezeNet achieves the worst value, which is 83.80%. Among pre-trained methods, although AlexNet has a closer performance to the proposed method, it is failed to provide the ability to outperform it. As a result of investigating specificity values, it can be clearly shown that the proposed method has a high-level classification capability in 2-class. For instance, whilst the specificity value of 97.65% is obtained with the proposed model, those of SqueezeNet, ShuffleNet, and AlexNet are calculated as being 95.20%, 93.30%, and 92.85%, respectively. The F1 values obtained from the pre-trained deep learning methods are obtained as being 84.84% for SqueezeNet, 91.34% for ShuffleNet, and 93.22% for AlexNet, respectively. The F1 value of the proposed method is the best, which is 97.32%. The confusion matrix for the proposed method is given in Fig. 7. When the confusion matrix is analyzed, 107 images were misclassified out of 4000, and an accuracy of 97.32% is achieved for 2-class.

To research the success of the proposed method in classification of faults from PV module images, the experiments are also performed for 11-class. The dataset obtained for the 11-class consists of 22,524 images for Cell, 15,456 images for Cell-Multi, 11,280 images for Cracking, 17,988 images for Diode, 2100 images for Diode-Multi, 2988 images for Hot-Spot, 2952 images for Hot-Spot-Multi, 9925 images for Offline-Module, 12,672 images for Shadowing, 2448 images for Soiling, and 19,668 images for Vegetation. In order to balance the dataset, the number of images in each fault class is equalized to the fault class with the least number of images. In this way, the problems that will arise from the unbalanced dataset are eliminated. The new dataset obtained for the 11-class consists of a total of 23,100 images, being equal in each fault class. Afterward, all deep learning methods are trained by using the new dataset. The metric results obtained from experiments are given in Table 4, where the highest metric values are marked in boldface. In addition, Fig. 8 is given to better show the obtained results. The classification performances of all methods are evaluated by means of the accuracy, precision, sensitivity, specificity, F1, and MCC. According to classification results in Table 4, the proposed method outperforms the pre-trained deep learning methods as it is capable of correctly classify 93.51% of the PV module faults.

As expected, the metric result values of the proposed method are very high because of its effective structure and balanced data. For instance, the accuracy, precision, sensitivity, specificity, F1, and MCC values of the proposed method are calculated as being 93.51%, 93.52%, 93.51%, 99.35%, 93.49%, and 92.86%, respectively. Among all the pre-trained deep learning methods, AlexNet provides the second best classification accuracy of 85.02%, precision of 85.36%, sensitivity of 85.02%, specificity of 98.50%, F1 of 84.60%, and MCC of 83.46%, respectively. Similar to 2-class classification results, SqueezeNet has the worst metric values, which are 75.15% for accuracy, 75.87% for precision, 75.15% for sensitivity, 97.52 for specificity, 74.50 for F1, and 72.65% for MCC, respectively. Moreover, the confusion matrix of the proposed method is presented in Fig. 9. The proposed method correctly predicts 2160 out of 2310 PV module images. For in-depth analysis for class-11, the performance of the proposed method is separately analyzed in terms of each fault. The obtained classification results are listed in Table 5.

As can be seen in the confusion matrix and Table 5, the Cell, Cell-Multi, and Vegetation classes give only less than 90% accuracy. While the network predicts 176 images as Cell, 18 images are only predicted as Cell-Multi. However, these classes represent the same anomalies. Cell class represents hot spot occurring with a square geometry in a single cell and Multi-Cell class represents the hot spot occurring with a square geometry in multiple cells. Therefore, a relatively low accuracy value is obtained. For the Vegetation, the accuracy is 86.19% and the highest negative prediction is against the Cell. The reason for the relatively

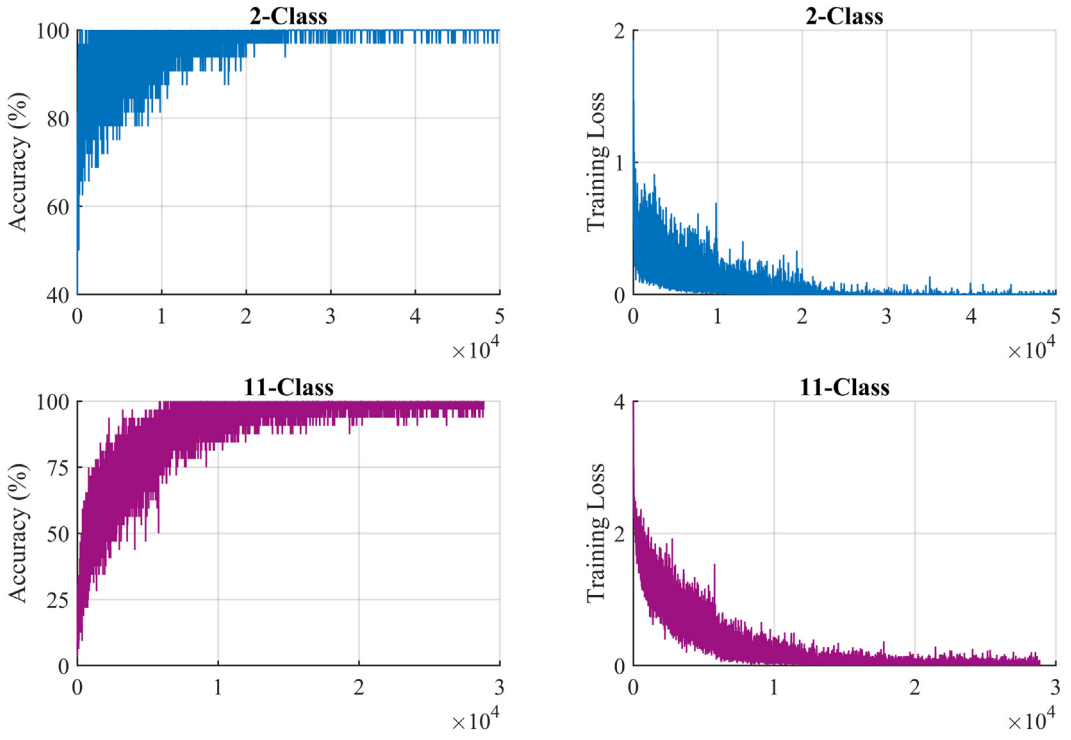

Fig. 6. Training progress of the multi-scale CNN for 2 and 11 class experiments.

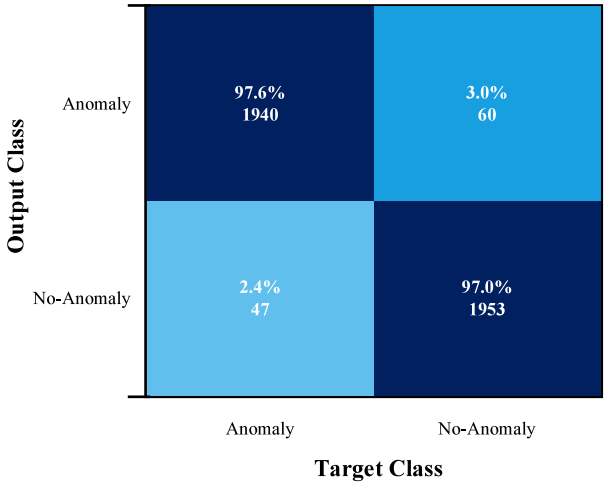

Fig. 7. The confusion matrix of the proposed method for 2-class.

low accuracy is due to the cell anomaly similarity of the vegetation. In addition, the proposed method provides the highest classification accuracy of 99.52% in Diode-Multi and Hot-Spot classes. While the lowest value in precision is in Cell class with 81.10%, the highest value is obtained in Diode-Multi class with 99.52%. The best results in sensitivity, specificity, F1, and MCC are in Diode-Multi class.

The activations in the different convolutions of the proposed method is given in Fig. 10. While Conv-1 and Conv-2 represent the first two convolutions, Convolutions 3–*i* present the parallel branches. By comparing the original input image with the areas of activation, it can be easily obtained which features the proposed method learns. In Fig. 10, first 64 channels are presented. The white pixels show strong positive activations and the black pixels indicate strong negative activations. In addition, white pixels in a channel describe the strongly activated channel at that position.

Table 5
The classification results of proposed method for each fault in 11-class.

Fault	Acc (%)	Pr (%)	Sn (%)	Sp (%)	F1 (%)	MCC (%)
Cell	83.80	81.10	83.80	98.04	82.43	80.66
Cell-Multi	81.90	84.31	81.90	98.47	83.09	81.43
Cracking	94.76	96.13	94.76	99.61	95.44	94.99
Diode	96.66	98.06	96.66	99.80	97.36	97.10
Diode-Multi	99.52	99.52	99.52	99.95	99.52	99.47
Hot-Spot	99.52	97.20	99.52	99.71	98.35	98.19
Hot-Spot-Multi	99.04	95.41	99.04	99.52	97.19	96.93
Offline-Module	96.66	94.85	96.66	99.47	95.75	95.33
Shadowing	96.19	93.08	96.19	99.28	94.61	94.08
Soiling	94.28	98.50	94.28	99.85	96.35	96.02
Vegetation	86.19	90.50	86.19	99.09	88.29	87.18
Overall	**93.51**	**93.52**	**93.51**	**99.35**	**93.49**	**92.86**

Figs. 11 and 12 show the t-distributed stochastic neighbor embedding (t-SNE) distributions of extracted features from the proposed method for 2-class and 11-class. Through the t-SNE, the distribution of the classes in each layer can be observed clearly. As can be seen from the Figures, the maps obtained from t-SNE contain some different points that are clustered with the wrong class in the first layers. In the maps in the last layers, each class is clustered in separate regions and very few wrong points are distributed in different clusters. When the clusters in the fc-3 layer of the proposed method are analyzed, it is seen that the distribution of the classes is quite better.

3.4. Analysis of improvement percentages

To highlight the classification performance of the proposed method, the improvement percentages are calculated over the pre-trained deep learning methods, namely, SqueezeNet, ShuffleNet, and AlexNet. The obtained improvement percentages are presented in Tables 6 and 7 for 2-class and 11-class. In addition, bar graphs are given in Fig. 13 for each metric to better observe the improvement percentages.

As can be seen from Tables 6 and 7, the proposed method significantly improves the classification performance of the pre-trained

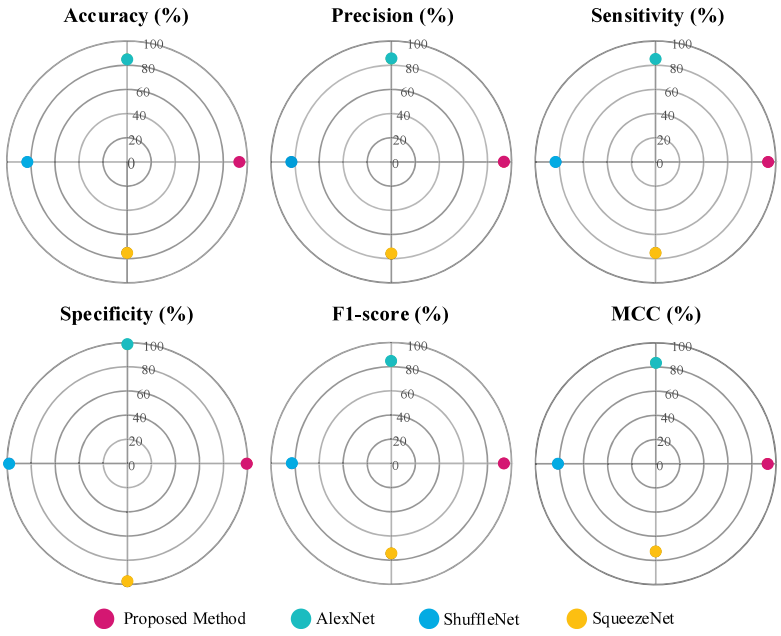

Fig. 8. The comparison of classification results of all methods for 11-class.

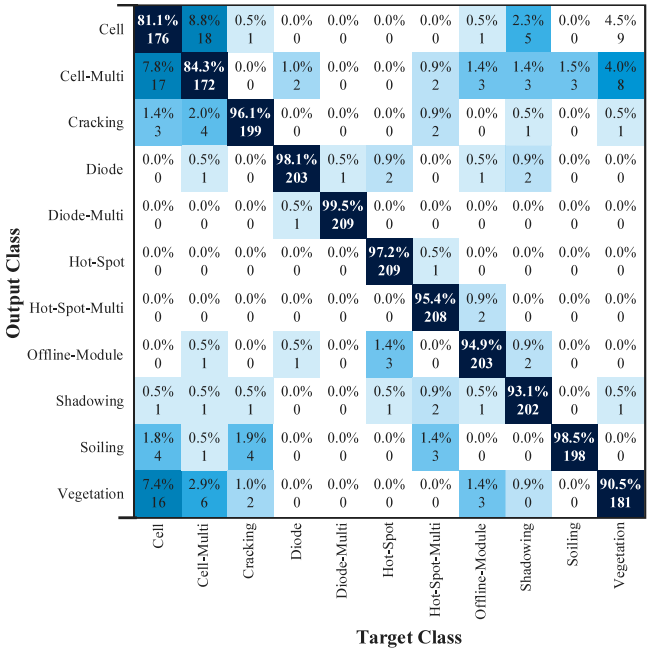

Fig. 9. The confusion matrix of the proposed method for 11-class.

Table 6
The improvement percentage results of each fault in 2-class.

Method	Acc (%)	Pr (%)	Sn (%)	Sp (%)	F1 (%)	MCC (%)
SquezeeNet	14.47	13.66	15.75	2.57	14.71	35.08
ShuffleNet	6.36	4.92	8.14	4.66	6.55	13.97
AlexNet	4.42	5.09	3.69	5.17	4.40	9.55

Table 7
The improvement percentage results of each fault in 11-class.

Method	Acc (%)	Pr (%)	Sn (%)	Sp (%)	F1 (%)	MCC (%)
SqueezeNet	24.43	23.26	24.43	1.88	25.49	27.82
ShuffleNet	12.74	12.74	12.74	1.08	12.99	14.42
AlexNet	9.99	9.56	9.99	0.86	10.51	11.26

deep learning methods. For instance, when analyzed to the improvement percentages in accuracy values for 2-class and 11-class, the proposed method improved the performance of SqueezeNet by 14.47% to 24.43%, ShuffleNet by 6.36% to 12.74%, and AlexNet by 4.42% to 9.99%, respectively. The highest precision improvements in both classes are achieved in SqueezeNet. For example, the precision values of SqueezeNet, ShuffleNet, and AlexNet are improved on by the proposed method by 13.66%, 4.92%, 5.09% for 2-class, and 23.26%, 12.74%, 9.56% for 11-class, respectively.

When compared the proposed method with SqueezeNet, ShuffleNet, and AlexNet, the improvement percentages in sensitivity values are calculated as being 15.75%, 8.14%, 3.69% for 2-class, and 24.43%, 12.74%, 9.99% for 11-class, respectively. Moreover, the proposed method led to 2.57%, 4.66%, 5.17%, and 1.88%, 1.08%, 0.86% improvements in specificity values for 2 and 11-class in comparison with SqueezeNet, ShuffleNet, and AlexNet, respectively. The proposed method gives rise to 4.40% for 2-class and 10.51% for 11-class improvements in F1 values in comparison with AlexNet, whilst improvements in F1 values for SqueezeNet and ShuffleNet were reported as 14.71% and 6.55% for 2-class, and 25.49% and 12.99% for 11-class, respectively. The improvement percentages in MCC values of the proposed method over SqueezeNet, ShuffleNet and AlexNet are calculated as 35.08%, 13.97%, 9.55% for 2-class, and 27.82%, 14.42%, 11.26% for 11-class, respectively. These results clearly indicate that the proposed multi-scale CNN model has not only the effectiveness and suitability classification results than pre-trained deep learning methods but also guarantees more reliable operation of PV systems.

3.5. Comparison between the proposed method and state-of-the-art methods

Trouble-free operation of PV systems is of great importance. If the module faults in PV systems are not detected in a timely manner, the generation of the system may be low. The early diagnosis of module faults in these systems can be associated with fast and accurate results of the image processing approaches. The CNN structures provide more reliable and better results than other methods in diagnosing these faults. Furthermore, the CNN methods can guarantee a powerful classification ability. Consequently, CNNs are widely used in the diagnosis of PV module faults because of their superior properties. In this paper,

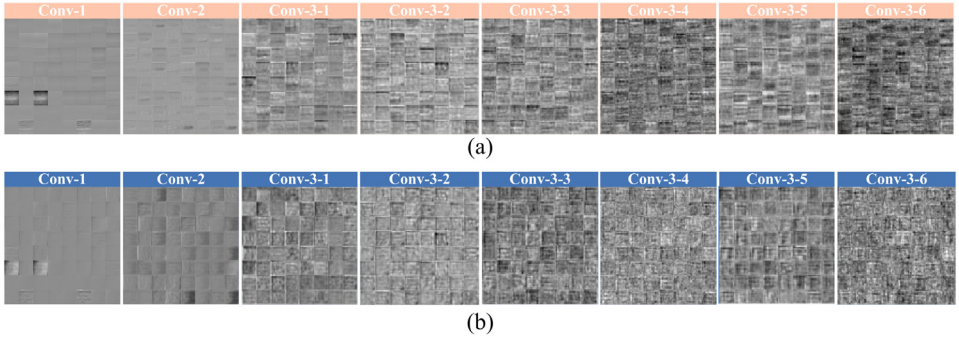

Fig. 10. The activations obtained from different convolutions. (a) 2-class, (b) 11-class.

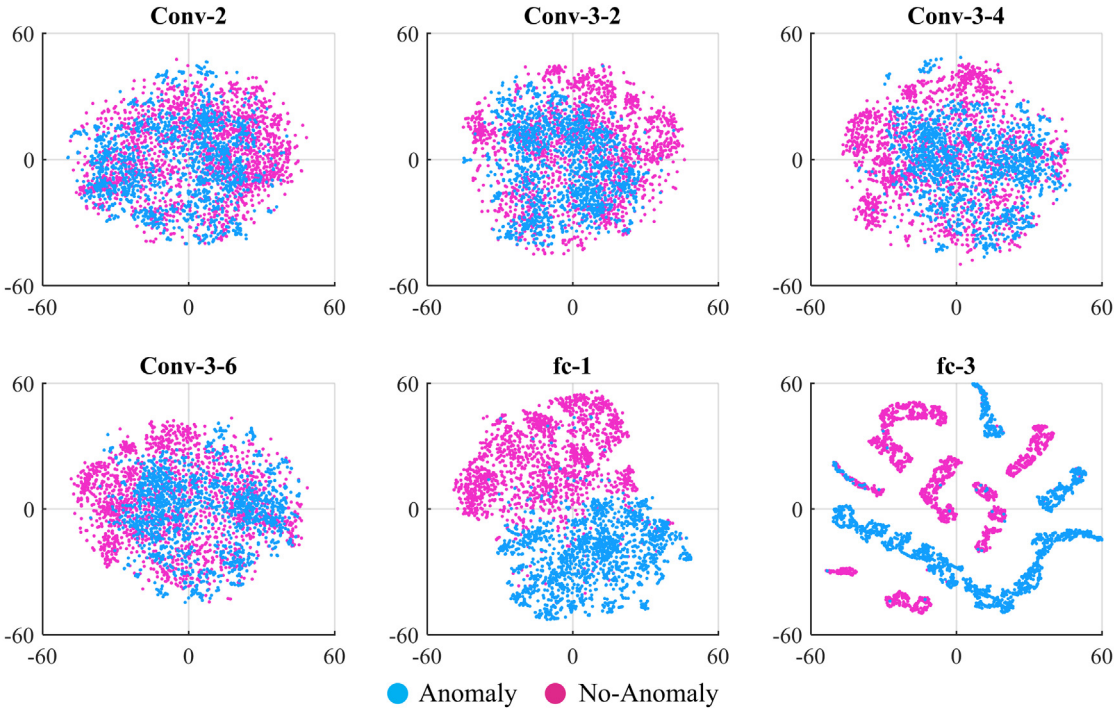

Fig. 11. The t-SNE view of extracted features from the convolution layers of the proposed method for 2-class.

Table 8
Comparison of the classification results of the related studies using the same dataset for 2-class (%).

Study	Year	Method	Acc	Pr	Sn	Sp	F1	MCC
Fonseca Alves et al.	2021	CNN	92.50	92.00	92.00	–	92.00	–
Le et al.	2021	Ensemble model	94.40	–	–	–	–	–
Proposed method	2021	CNN	**97.32**	**97.63**	**97.00**	**97.65**	**97.32**	**94.65**

we proposed an efficient fault diagnosis method for PV module faults. Comparisons are realized with studies using the same dataset to fairly assess the classification ability of the proposed method. Tables 8 and 9 show the classification results of the related studies for 2-class and multi-class.

According to Tables 8 and 9, Fonseca Alves et al. (2021) proposed a CNN structure to classify faults in PV modules. The authors obtained a balanced dataset using undersampling and oversampling methods. They considered four scenarios to test the classification performance of the proposed method. The overall accuracy, precision, sensitivity, and F1 values obtained from this study for 2-class can be given as 92.50%, 92.00%, 92.00%, and 92.00%, respectively. Moreover, the authors stated that the proposed method provided 66.43% accuracy for the 11-class. Le et al. (2021) presented a deep neural network structure that uses residual network structure and ensemble technique to classify faults in PV modules. After the network designing, the authors tried different transformations to augment the dataset, thus aiming to obtain the best classification results. Moreover, they obtained the number of the optimal filters by testing the raw and the augmented dataset on the proposed method with different filter numbers. Their proposed method has 94.40% of accuracy for 2-class and 85.90% of accuracy for 12-class, respectively.

When the metric results given in Tables 8 and 9 are analyzed, the proposed method outperforms better than other studies using the same dataset in diagnosing faults in the PV modules. When the classification results obtained from three studies are compared in terms of accuracy values, multi-scale CNN has the highest accuracy values, which are 97.32% for 2-class and 93.51% for 11-class. In addition, the proposed method is improved the accuracy values obtained from other methods by 5.21% and 3.09% for 2-class, respectively. The accuracy values in

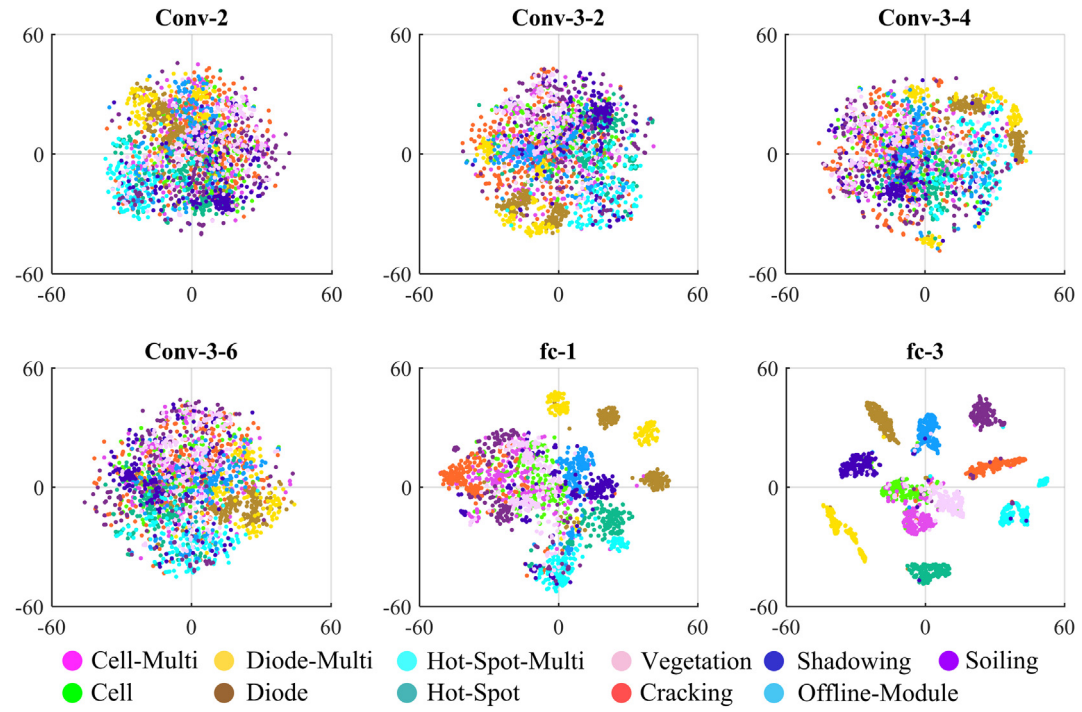

Fig. 12. The t-SNE view of extracted features from the convolution layers of proposed method for 11-class.

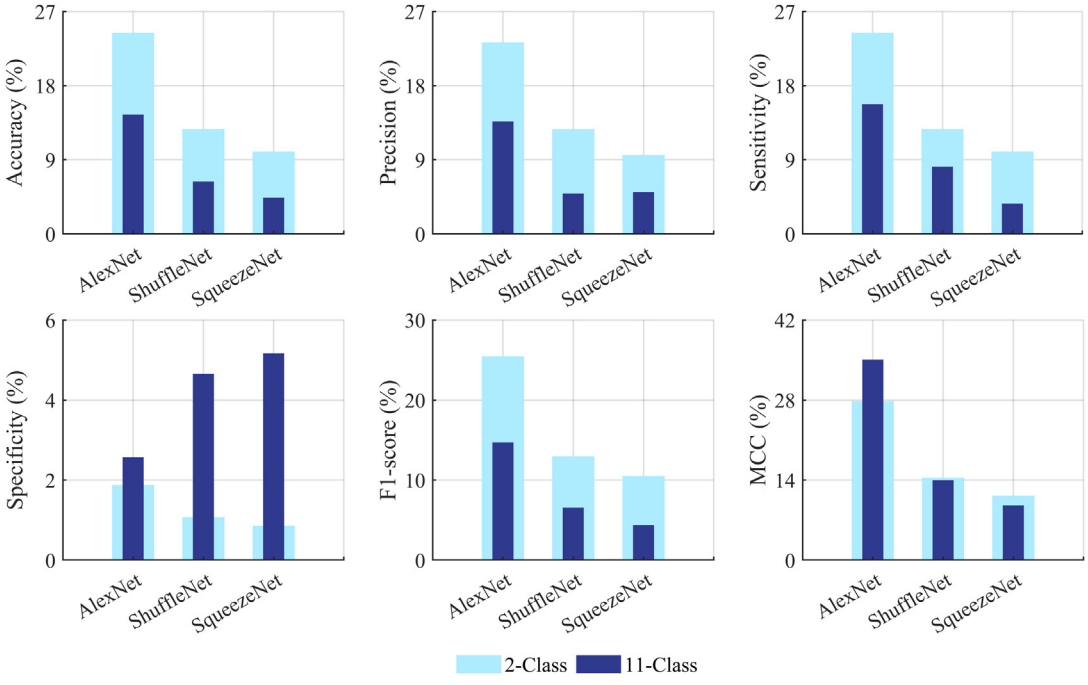

Fig. 13. The bar graphs of improvement percentages for 2 and 11-classes.

Table 9
Comparison of the classification results of the related studies using the same dataset for multi-class.

Study	Year	Method	Class number	Acc (%)
Fonseca Alves et al.	2021	CNN	11	66.43
Le et al.	2021	Ensemble model	12	85.90
Proposed method	2021	CNN	11	**93.51**

studies for multi-class are improved as 40.76% and 8.86%, respectively. As can be easily seen from these results, the proposed multi-scale CNN provides a quite satisfactory classification performance despite the increase in the number of classes.

4. Conclusion

In this study, a powerful deep learning method is proposed to classify faults in PV modules. First, the IR images collected from different solar power plants are separated according to different fault classes such as Cell, Cell-Multi, Cracking, Diode, Diode-Multi, Hot-Spot, Hot-Spot-Multi, Offline-Module, Shadowing, Soiling, Vegetation,

and No-Anomaly. Due to the low number of some fault images, data augmentation is made to increase the classification success of the proposed method. After all processes, the obtained PV module fault images are divided into 2 and 11-classes. The whole fault images in both classes are adjusted to be equal in number, thus obtaining a balanced dataset. The classification performance and capability of the proposed method are compared to pre-trained deep learning methods such as SqueezeNet, ShuffleNet, and AlexNet. When the metric results of the methods are analyzed, the accuracy values of the proposed CNN method are calculated as 97.32% for 2-class and 93.51% for 11-class. AlexNet is provided the second best accuracy values, which are 93.20% for 2-class and 85.02% for 11-class. In addition, the proposed method is significantly improved the classification results obtained from pre-trained deep learning methods. For instance, the average improvement percentages in accuracy values for 2-class and 11-class are ranged from 4.42% to 14.47% and 9.99% to 24.43%, respectively. When all the obtained results are evaluated, it is thought that the proposed method can not only correctly detect and classify the faults in PV modules, but also can play an important role in the more efficient operation of PV systems.

In future works, the proposed CNN method could be improved with an effective optimization algorithm to obtain a more robust anomaly classification performance. In addition, the proposed method could be utilized for fault detection of different RES types.

CRediT authorship contribution statement

Deniz Korkmaz: Conceptualization, Data curation, Formal analysis, Investigation, Methodology, Hardware, Visualization, Roles/Writing – original draft. **Hakan Acikgoz:** Conceptualization, Data curation, Formal analysis, Investigation, Methodology, Hardware, Visualization, Roles/Writing – original draft.

Declaration of competing interest

The authors declare that they have no known competing financial interests or personal relationships that could have appeared to influence the work reported in this paper.

References

Acikgoz, H., 2022. A novel approach based on integration of convolutional neural networks and deep feature selection for short-term solar radiation forecasting. Appl. Energy 305, 117912. http://dx.doi.org/10.1016/j.apenergy.2021.117912.

Ahmed, W., Hanif, A., Kallu, K.D., Kouzani, A.Z., Ali, M.U., Zafar, A., 2021. Photovoltaic panels classification using isolated and transfer learned deep neural models using infrared thermographic images. Sensors 21, 1–14. http://dx.doi.org/10.3390/s21165668.

Ali, M.U., Khan, H.F., Masud, M., Kallu, K.D., Zafar, A., 2020. A machine learning framework to identify the hotspot in photovoltaic module using infrared thermography. Sol. Energy 208, 643–651. http://dx.doi.org/10.1016/j.solener.2020.08.027.

Aziz, F., Haq, A.Ul., Ahmad, S., Mahmoud, Y., Jalal, M., Ali, U., 2020. A novel convolutional neural network-based approach for fault classification in photovoltaic arrays. IEEE Access 8, 41889–41904. http://dx.doi.org/10.1109/ACCESS.2020.2977116.

Ballester, P., Araujo, R.M., 2016. On the performance of googlenet and alexnet applied to sketches. In: 30th AAAI Conf. Artif. Intell. AAAI 2016. pp. 1124–1128.

Bommes, L., Pickel, T., Buerhop-Lutz, C., Hauch, J., Brabec, C., Peters, I.M., 2021. Computer vision tool for detection, mapping, and fault classification of photovoltaics modules in aerial IR videos. Prog. Photovolt. Res. Appl. 123, 6–1251. http://dx.doi.org/10.1002/pip.3448.

Buda, M., Maki, A., Mazurowski, M.A., 2018. A systematic study of the class imbalance problem in convolutional neural networks. Neural Netw. 106, 249–259. http://dx.doi.org/10.1016/j.neunet.2018.07.011.

Cai, B., Hao, K., Wang, Z., Yang, C., Kong, X., Liu, Z., Ji, R., Liu, Y., 2021. Data-driven early fault diagnostic methodology of permanent magnet synchronous motor. Expert Syst. Appl. 177, 115000. http://dx.doi.org/10.1016/j.eswa.2021.115000.

Cai, B., Sun, X., Wang, J., Yang, C., Wang, Z., Kong, X., Liu, Z., Liu, Y., 2020. Fault detection and diagnostic method of diesel engine by combining rule-based algorithm and BNs/BPNNs. J. Manuf. Syst. 57, 148–157. http://dx.doi.org/10.1016/j.jmsy.2020.09.001.

Cai, B., Wang, Z., Zhu, H., Liu, Y., Hao, K., Yang, Z., Ren, Y., Feng, Q., Liu, Z., 2022. Artificial intelligence enhanced two-stage hybrid fault prognosis methodology of PMSM. IEEE Trans. Ind. Inform. 1–12. http://dx.doi.org/10.1109/TII.2021.3128245.

Cipriani, G., D'Amico, A., Guarino, S., Manno, D., Traverso, M., Di Dio, V., 2020. Convolutional neural network for dust and hotspot classification in PV modules. Energies 13. http://dx.doi.org/10.3390/en13236357.

Deepak, S., Ameer, P.M., 2019. Brain tumor classification using deep CNN features via transfer learning. Comput. Biol. Med. 111, 103345. http://dx.doi.org/10.1016/j.compbiomed.2019.103345.

Dhibi, K., Fezai, R., Mansouri, M., Trabelsi, M., Kouadri, A., Bouzara, K., Nounou, H., Nounou, M., 2020. Reduced kernel random forest technique for fault detection and classification in grid-tied PV systems. IEEE J. Photovolt. 10, 1864–1871. http://dx.doi.org/10.1109/JPHOTOV.2020.3011068.

Dunderdale, C., Brettenny, W., Clohessy, C., van Dyk, E.E., 2020. Photovoltaic defect classification through thermal infrared imaging using a machine learning approach. Prog. Photovolt. Res. Appl. 28, 177–188. http://dx.doi.org/10.1002/pip.3191.

Fernández, A., Usamentiaga, R., de Arquer, P., Fernández, M.Á., Fernández, D., Carús, J.L., Fernández, M., 2020. Robust detection, classification and localization of defects in large photovoltaic plants based on unmanned aerial vehicles and infrared thermography. Appl. Sci. 10. http://dx.doi.org/10.3390/app10175948.

Fonseca Alves, R.H., Deus Júnior, G.A.de, Marra, E.G., Lemos, R.P., 2021. Automatic fault classification in photovoltaic modules using convolutional neural networks. Renew. Energy 179, 502–516. http://dx.doi.org/10.1016/j.renene.2021.07.070.

Han, D., Liu, Q., Fan, W., 2018. A new image classification method using CNN transfer learning and web data augmentation. Expert Syst. Appl. 95, 43–56. http://dx.doi.org/10.1016/j.eswa.2017.11.028.

Haque, A., Bharath, K.V.S., Khan, M.A., Khan, I., Jaffery, Z.A., 2019. Fault diagnosis of photovoltaic modules. Energy Sci. Eng. 7, 622–644. http://dx.doi.org/10.1002/ese3.255.

Huerta Herraiz, Á., Pliego Marugán, A., García Márquez, F.P., 2020. Photovoltaic plant condition monitoring using thermal images analysis by convolutional neural network-based structure. Renew. Energy 153, 334–348. http://dx.doi.org/10.1016/j.renene.2020.01.148.

Iandola, F.N., Han, S., Moskewicz, M.W., Ashraf, K., Dally, W.J., Keutzer, K., 2016. SqueezeNet: AlexNet-Level accuracy with 50x fewer parameters and <0.5MB model size. pp. 1–13, arxiv:1602.07360.

Kirsten Vidal de Oliveira, A., Aghaei, M., Rüther, R., 2020. Aerial infrared thermography for low-cost and fast fault detection in utility-scale PV power plants. Sol. Energy 211, 712–724. http://dx.doi.org/10.1016/j.solener.2020.09.066.

Korkmaz, D., 2021. SolarNet: A Hybrid reliable model based on convolutional neural network and variational mode decomposition for hourly photovoltaic power forecasting. Appl. Energy 300, 117410. http://dx.doi.org/10.1016/j.apenergy.2021.117410.

Korkmaz, D., Acikgoz, H., Yildiz, C., 2021. A novel short-term photovoltaic power forecasting approach based on deep convolutional neural network. Int. J. Green Energy 1–15. http://dx.doi.org/10.1080/15435075.2021.1875474.

Le, M., Van Su, L., Dang Khoa, N., Dao, V.D., Ngoc Hung, V., Hong Ha Thi, V., 2021. Remote anomaly detection and classification of solar photovoltaic modules based on deep neural network. Sustain. Energy Technol. Assess. 48, 101545. http://dx.doi.org/10.1016/j.seta.2021.101545.

Li, B., Delpha, C., Diallo, D., Migan-Dubois, A., 2021. Application of artificial neural networks to photovoltaic fault detection and diagnosis: A review. Renew. Sustain. Energy Rev. 138. http://dx.doi.org/10.1016/j.rser.2020.110512.

Liu, J., Guo, F., Gao, H., Huang, Z., Zhang, Y., Zhou, H., 2021. Image classification method on class imbalance datasets using multi-scale CNN and two-stage transfer learning. Neural Comput. Appl. 33, 14179–14197. http://dx.doi.org/10.1007/s00521-021-06066-8.

Manno, D., Cipriani, G., Ciulla, G., Di Dio, V., Guarino, S., Lo Brano, V., 2021. Deep learning strategies for automatic fault diagnosis in photovoltaic systems by thermographic images. Energy Convers. Manage. 241, 114315. http://dx.doi.org/10.1016/j.enconman.2021.114315.

Matthew, M., Edward, O., Vadhavkar, N., 2020. Infrared solar module dataset for anomaly detection. Int. Conf. Learn. Represent. 1–5.

Otamendi, U., Martinez, I., Quartulli, M., Olaizola, I.G., Viles, E., Cambarau, W., 2021. Segmentation of cell-level anomalies in electroluminescence images of photovoltaic modules. Sol. Energy 220, 914–926. http://dx.doi.org/10.1016/j.solener.2021.03.058.

Pan, S.J., Yang, Q., 2010. A survey on transfer learning. IEEE Trans. Knowl. Data Eng. 22, 1345–1359. http://dx.doi.org/10.1109/TKDE.2009.191.

Rahaman, S.A., Urmee, T., Parlevliet, D.A., 2020. PV System defects identification using remotely piloted aircraft (RPA) based infrared (IR) imaging: A review. Sol. Energy 206, 579–595. http://dx.doi.org/10.1016/j.solener.2020.06.014.

Rico Espinosa, A., Bressan, M., Giraldo, L.F., 2020. Failure signature classification in solar photovoltaic plants using RGB images and convolutional neural networks. Renew. Energy 162, 249–256. http://dx.doi.org/10.1016/j.renene.2020.07.154.

Shorten, C., Khoshgoftaar, T.M., 2019. A survey on image data augmentation for deep learning. J. Big Data 6, 1–48. http://dx.doi.org/10.1186/s40537-019-0197-0.

Tang, W., Yang, Q., Xiong, K., Yan, W., 2020. Deep learning based automatic defect identification of photovoltaic module using electroluminescence images. Sol. Energy 201, 453–460. http://dx.doi.org/10.1016/j.solener.2020.03.049.

Wang, Q., Paynabar, K., Pacella, M., 2021. Online automatic anomaly detection for photovoltaic systems using thermography imaging and low rank matrix decomposition. J. Qual. Technol. 1–14. http://dx.doi.org/10.1080/00224065.2021.1948372.

Zhang, X., Zhou, X., Lin, M., Sun, J., 2018. ShuffleNet: AN extremely efficient convolutional neural network for mobile devices. In: Black Stud. Read. 2018 IEEE/. pp. 6848–6856. http://dx.doi.org/10.1109/CVPR.2018.00716.